All-Solid-State Symmetric Supercapacitor Based on Co_3O_4 Nanoparticles on Vertically Aligned Graphene

Qingyu Liao,[†,‡] Na Li,[†,‡] Shuaixing Jin,[†,‡] Guowei Yang,[‡] and Chengxin Wang*[,†,‡]

[†]The Key Laboratory of Low-Carbon Chemistry & Energy Conservation of Guangdong Province and [‡]State Key Laboratory of Optoelectronic Materials and Technologies, School of Physics Science and Engineering, Sun Yat-sen (Zhongshan) University, Guangzhou 510275, People's Republic of China

ABSTRACT We have synthesized the hybrid supercapacitor electrode of Co_3O_4 nanoparticles on vertically aligned graphene nanosheets (VAGNs) supported by carbon fabric. The VAGN served as an excellent backbone together with the carbon fabric, enhancing composites to a high specific capacitance of 3480 F/g, approaching the theoretical value (3560 F/g). A highly flexible all-solid-state symmetric supercapacitor device was fabricated by two pieces of our Co_3O_4/VAGN/carbon fabric hybrid electrode. The device is suitable for different bending angles and delivers a high capacitance (580 F/g), good cycling ability (86.2% capacitance retention after 20 000 cycles), high energy density (80 Wh/kg), and high power density (20 kW/kg at 27 Wh/kg). These excellent electrochemical performances, as a result of the particular structure of VAGN and the flexibility of the carbon fabric, suggest that these composites have an enormous potential in energy application.

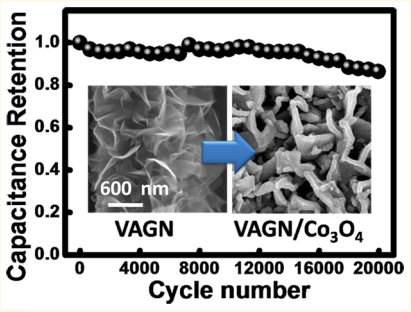

KEYWORDS: energy storage · graphene · cobalt oxides · all-solid-state supercapacitors

The demand for power sources of portable electronic devices has increased in recent years due to the large proliferation of e-readers, tablets, and smartphones. Therefore, it is critical to miniature the energy device without jeopardizing its power capacity. Supercapacitors stand out among other candidates because of their higher power density, cycle efficiency, and charge/discharge rate.[1] There are two types of supercapacitors based on the energy storage mechanism: electrical double-layer capacitors (EDLCs) and pseudocapacitors. Many efforts have been made to fabricate EDLCs with carbon-based materials such as carbon nanotubes[2] and reduced graphene oxide.[3] This type of supercapacitor stores electrical energy by electrostatic accumulation of charges in the electric double-layer near the electrode/electrolyte interfaces.[4] Additionally, transition metal oxides, *e.g.*, MnO_2,[5] RuO,[6] and NiO,[7] have been used to build pseudocapcitors. These pseudocapacitors, taking advantage of the reversible Faradaic reactions occurring at the electrode surface, offer better electrochemical performances than the EDLCs.[4] Among these transition metal oxide candiates, Co_3O_4 is considered to be ideal due to its high theoretical capacitance (3560 F/g), environmental friendliness, and good electrochemical performance.[8] However, in many cases, the observed specific capacitances are far lower than the theoretical value.[9,10] Thus, it is still a challenge to fabricate a Co_3O_4-based supercapacitor with high specific capacitances.

The low electronic conductivity of Co_3O_4 limits the performance of supercapacitors by hindering the transfer of electrons.[11] In order to overcome this limitation, much work has focused on the incorporation of Co_3O_4 into highly conductive nanostructured carbons.[8,11] Graphene nanosheets (GNSs) are an excellent backbone to hold these transition metal oxides, because of their outstanding feature of high conductivity and specific surface.[3,12] However, the strong $\pi-\pi$ interactions and the van der Waals force between the planar basal planes cause the normal GNSs to restack themselves.[13] These drawbacks can be overcome by employing a vertically aligned graphene nanosheet (VAGN) with its bottom fixed to the surface of the substrate. Thus, the space between each pair of sheets

* Address correspondence to (C. X. Wang) wchengx@mail.sysu.edu.cn.

Received for review February 4, 2015 and accepted May 4, 2015.

Published online May 04, 2015
10.1021/acsnano.5b00821

can be maintained during the subsequent procedures. What is more, the open space of the GNS reduces the internal resistance and facilitates the diffusion of electrolyte to the inner part of the electrode when assembled to a supercapcitor.[8]

Conventionally, electrodes are directly immersed into a solution containing Na_2SO_4, H_2SO_4, or KOH for liquid-electrolyte-based supercapacitors. As a result, these capacitors are not feasible options for electronic application because it is very difficult to shelter the other elements from the liquid electrolyte and to have flexibility.[3] Recently, all-solid-state supercapacitors based on carbon fabric (CF) have been explored extensively to meet the demand for flexible and wearable electronic devices.[14] The electrolyte of the all-solid-state supercapacitors is not as mobile as the liquid solution, so it can be easily separated from other parts of the device. Moreover, as a characteristic of carbon fabric, the supercapacitors can be easily fabricated to bend or twist.[15]

Here, we combined the VAGN and the carbon fabric to fabricate a supercapacitor electrode with Co_3O_4 nanoparticles. The VAGN together with the carbon fabric served as the backbone and current collector. The Co_3O_4 nanoparticles of ~5 nm were deposited on the VAGN *via* a facile hydrothermal method without breaking the specific structure of the VAGN. In the liquid-electrolyte-based three-electrode test, Co_3O_4 reaches a high specific capacitance of up to 3482 F/g obtained in a 2 M KOH aqueous solution. In addition, we also made the all-solid-state symmetric supercapacitor by assembling two pieces of the as-made electrodes. The fabricated supercapacitor exhibits an outstanding electrochemical performance with the highest energy density of 80 Wh/kg at a power density of 0.5 kW/kg and highest power density of 20 kW/kg at a energy density of 27 Wh/kg. The device demonstrates an excellent flexibility without significantly sacrificing the electrochemical performance when bent to 150 degrees. The capacitance retention is 86.3% after 20 000 cycles at 20 A/g.

RESULTS AND DISCUSSION

The flexible electrode was fabricated through a two-step approach. First, the VAGNs were synthesized on the carbon fabric (Scheme 1b). The carbon fabric was employed as the current collector along with the VAGN. The VAGN has a high nitrogen Brunauer–Emmett–Teller specific surface area of ~1800 m^2/g (Figure S1), indicating it to be an ideal backbone. Second, the Co_3O_4 nanoparticles were deposited onto the VAGN by a hydrothermal process with cobalt acetate ($Co(CH_3COO)_2$),[16] as shown in Scheme 1c (the details of the experiment are provided in the Experimental Section). By controlling the amount of cobalt acetate in the hydrothermal step, we made various samples with low, medium, and high mass loading content of Co_3O_4, named Co_3O_4-L, Co_3O_4-M, and Co_3O_4-H, respectively. The Co_3O_4-L, Co_3O_4-M, and Co_3O_4-H contained 25, 50, and 100 μg of Co_3O_4, respectively. The structures and morphologies of the composites were examined by scanning electron microscopy (SEM) and transmission electron microscopy (TEM). Figure 1a and b show the low- and high-resolution SEM images of the obtained VAGN/CF composites, respectively. The VAGN has been synthesized on each fiber, keeping a distance around 300 nm between each pair of neighboring sheets. The whole surface of each carbon fiber is totally covered by the graphene sheets. Figure 1c shows high-resolution SEM images of the Co_3O_4-H composite. The sample demonstrates analogous morphology with the VAGN. As expected, the specific structure of the VAGN has not been changed during the hydrothermal and following annealing step. The thickness of each sheet has increased to ~50 nm at Co_3O_4-H, which is evidence for the deposition of Co_3O_4. The existence of porous Co_3O_4 nanoparticles was further confirmed by TEM, as shown in Figure 2. For Co_3O_4-H, the surface of the VAGN was almost completely covered by Co_3O_4 nanoparticles with a grain size of around 5 nm (Figure 2a), and few particles were free of the VAGN. Figure 2b demonstrates that the Co_3O_4 nanoparticles are anchored to both sides of the VAGN in Co_3O_4-L. The graphene sheet is even a little deformed by the crowded nanoparticles. Noteworthy, the TEM of Co_3O_4-L is not much different from Co_3O_4-H, comparing Figure 2b with Figure 2a. Part of the area is not covered by the nanoparticles due to the low loading amount. This may result in the different behavior in the electrochemical test. The high-resolution TEM image further reveals the lattice fringes showing an interplanar spacing of 0.244 and 0.202 nm, corresponding to the (311) and (400) planes of the face-centered-cubic phase of Co_3O_4 (space group: *Fd*3*m* (227), JCPDS card no. 42-1467), respectively.

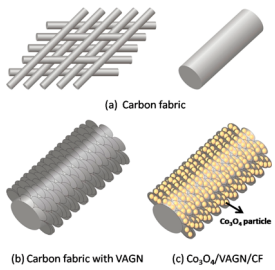

Scheme 1. Schematic illustration of the fabrication process and architecture of (a) carbon fabric, (b) the deposition of VAGN onto the carbon fabric, and (c) the deposition of Co_3O_4 nanoparticles onto the carbon fabric with VAGN.

Figure 3a shows the X-ray powder diffraction of the sample. All of the peaks of the composites coincide with those from the cubic phase Co_3O_4 in both position and relative intensities, except the peak at $2\theta = 26°$ from the VAGN/CF.[17] No other peaks presented indicate a high purity. The oxidation state of Co_3O_4 was characterized by X-ray photoelectron spectroscopy (XPS),

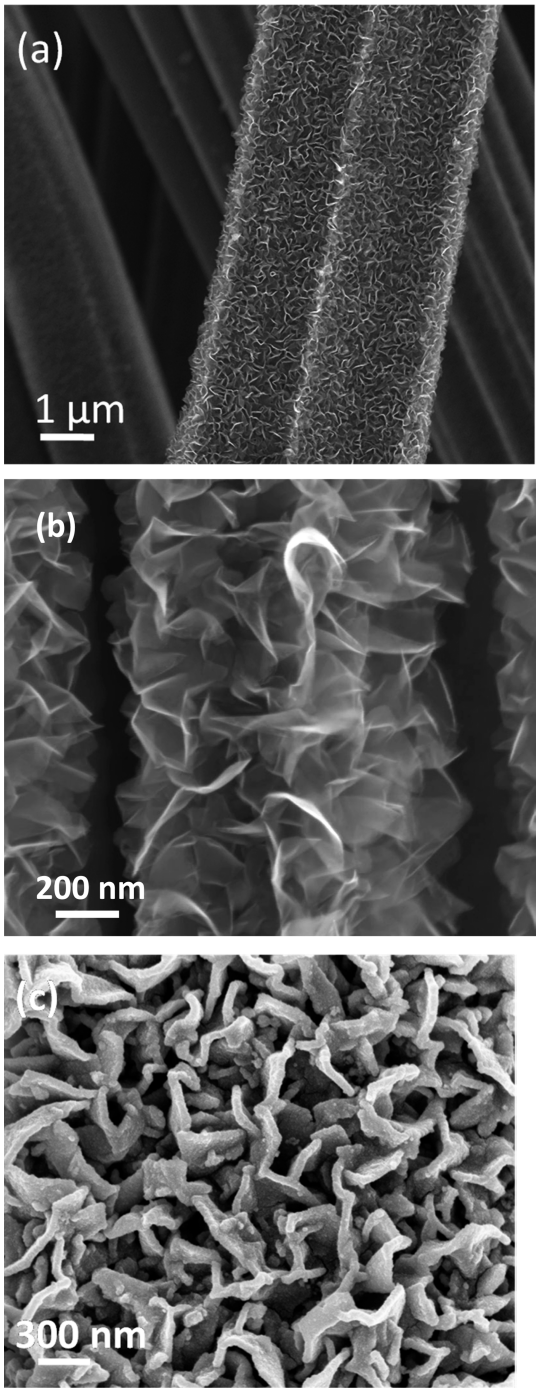

Figure 1. (a) Low-resolution SEM images of the VAGN, (b) high-resolution SEM images of the VAGN, and (c) high-resolution SEM image of Co_3O_4-H.

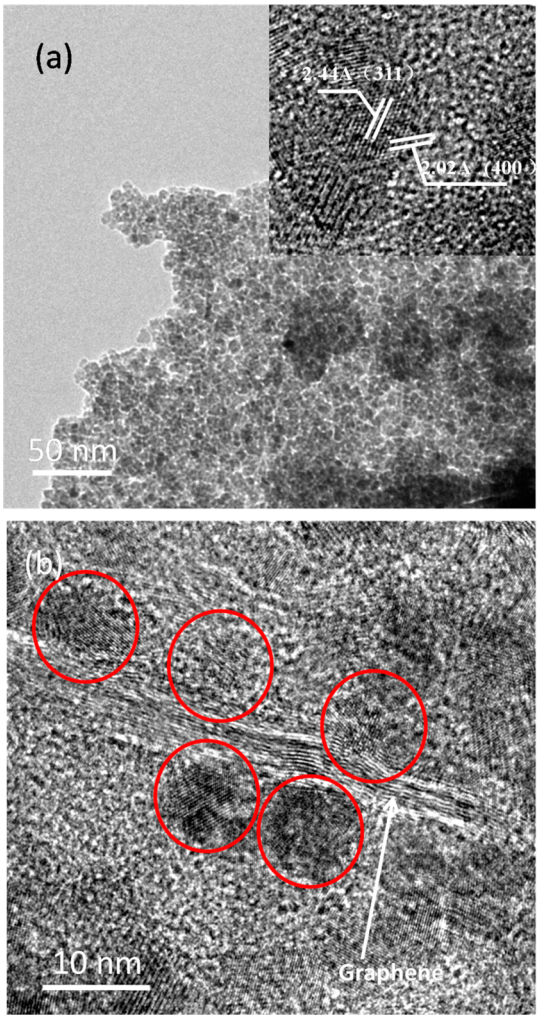

Figure 2. (a) Low- and high-resolution TEM images of Co_3O_4-H and (b) high-resolution TEM images of the VAGN and Co_3O_4 particles.

as shown in Figure 3b. The two peaks at 780.1 and 794.9 eV correspond to the Co $2p_{3/2}$ and Co $2p_{1/2}$ spin−orbit peaks of Co_3O_4, respectively.[18] The two shakeup satellite peaks located around 788 and 803 eV are also characteristic of Co_3O_4, in good agreement with the former reports.[18,19] This result is well consistent with that of XRD and the high-resolution TEM analysis.

To examine the electronic properties of the prepared Co_3O_4-based electrodes, we performed cyclic voltammetry (CV) measurements using a three-electrode test in 2 M KOH solution at the scan rate of 1−200 mV/s. The potential window is chosen from 0.25 to 0.75 V *vs* the Hg/HgO reference electrode. Figure 4a shows the CV plots of various electrodes at a scan rate of 50 mV/s. The electrode of VAGN/CF demonstrates a very low electric current response compared with the Co_3O_4-based electrode. Consequently, the contribution from VAGN/CF is neglected when evaluating the performance of the electrode. On the other hand, the three Co_3O_4-based electrodes share an analogous shape of the CV plot. The redox peaks are in evidence in the CV plots of the Co_3O_4 composite, indicating that the capacitance of Co_3O_4 mainly results from pseudocapacitance rather than the double-layer capacitance.[20] This is because the electric double-layer capacitance always gives a CV curve close to an ideal rectangular shape, while the pseudocapacitance has anodic and cathodic peaks from the corresponding redox reaction.[20] The reaction of the conversion in the electrolyte between different cobalt

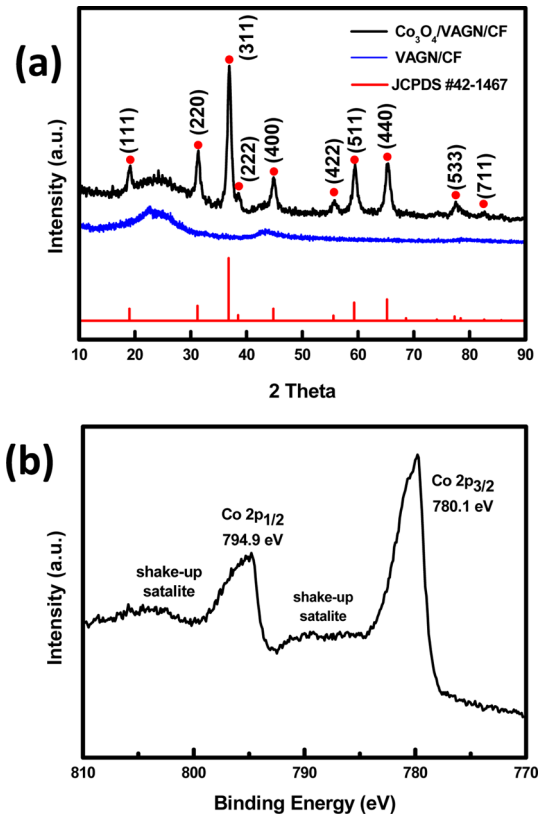

Figure 3. (a) XRD patterns of Co_3O_4/VAGN/CF and (b) Co 2p core-level XPS spectrum of Co_3O_4/VAGN/CF.

oxidation states can be proposed as follows:[20]

Reversible redox 1:

$$Co_3O_4 + OH^- + H_2O \leftrightarrow 3CoOOH + e^-$$

Reversible redox 2:

$$CoOOH + OH^- \leftrightarrow CoO_2 + H_2O + e^-$$

In Figure 4a, it is clear that two cathodic peaks can be found at around 0.45 and 0.52 V, corresponding to redox 2 and redox 1, respectively. However, only one anodic peak can be detected around 0.62 V at the same time. Previous reports gave a similar result.[20,21] The explanation for the disappearance of an anodic peak is that the product of redox 1, CoOOH, simultaneously undergoes further oxidation to CoO_2 in redox 2.[22] Thus, these two anodic peaks are so close that they could not be distinguished.

Figure 4b shows a CV chart of Co_3O_4-H. The increasing scan rate does not influence the shape of the CV curves significantly, indicating the good electron conduction in the host materials.[23] The anodic peaks shift to higher potential while the cathodic peaks shift to lower potential with increasing the scan rate, which is a result of the limitation of the ion diffusion rate to satisfy electronic neutralization during the redox reaction.[20] At the highest scan rate, the voltage window is not even wide enough to complete the redox reaction judging by the incomplete anodic peak, but the CV curve still shows

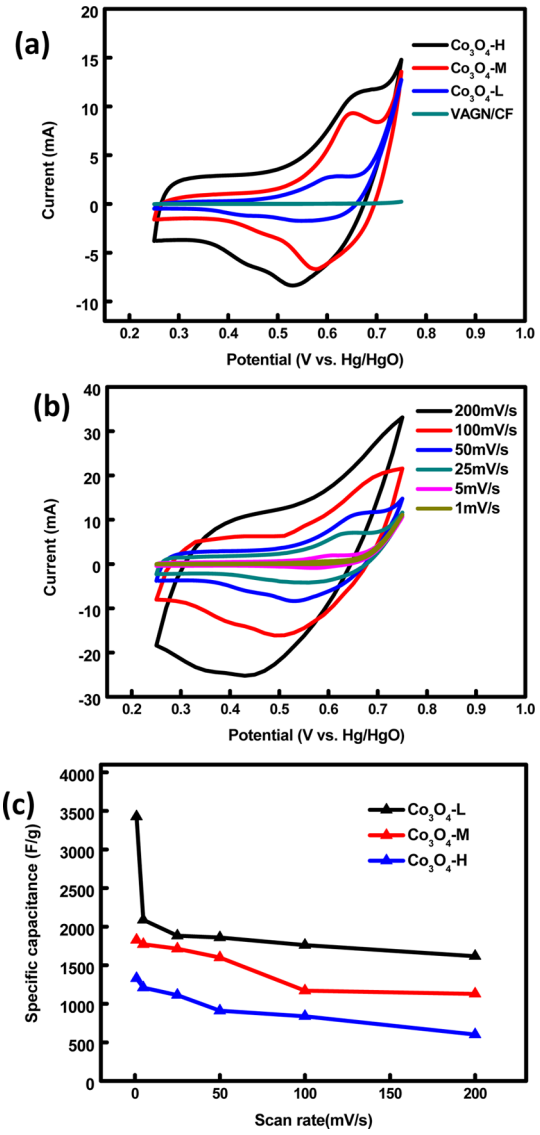

Figure 4. (a) CVs of VAGN and various Co_3O_4 composites at a scan rate of 50 mV/s, (b) CVs of the Co_3O_4-L electrode at scan rates from 1 to 200 mV/s, and (c) specific capacitance *vs* scan rate for various Co_3O_4 composites.

a pair of redox shapes, suggesting that the Co_3O_4-based electrodes were favorable for fast redox reactions.[12]

Figure 4c demonstrates specific capacitance (C_{sp}) as a function of the mass of Co_3O_4 and the scan rate. The highest C_{sp} is 3482 F/g at 1 mV/s of Co_3O_4-L, which is close to the theoretical value (3560 F/g) and higher than those in previous reports.[8,17,24] For the composites Co_3O_4-M and Co_3O_4-H, C_{sp} reached 1828 and 1330 F/g, respectively. The decreasing of C_{sp} as the amount increases is consistent with prior reports.[13,15,19] For Co_3O_4-L, each particle can take part in the redox reaction without congregating, as shown in Figure 2b, while for Co_3O_4-M and Co_3O_4-H, the surface area of the VAGN has been stretched to its limit with the crowded nanoparticles. As a consequence, some particles may not participate in the electrochemical process taking place at the interface of the electrolyte and

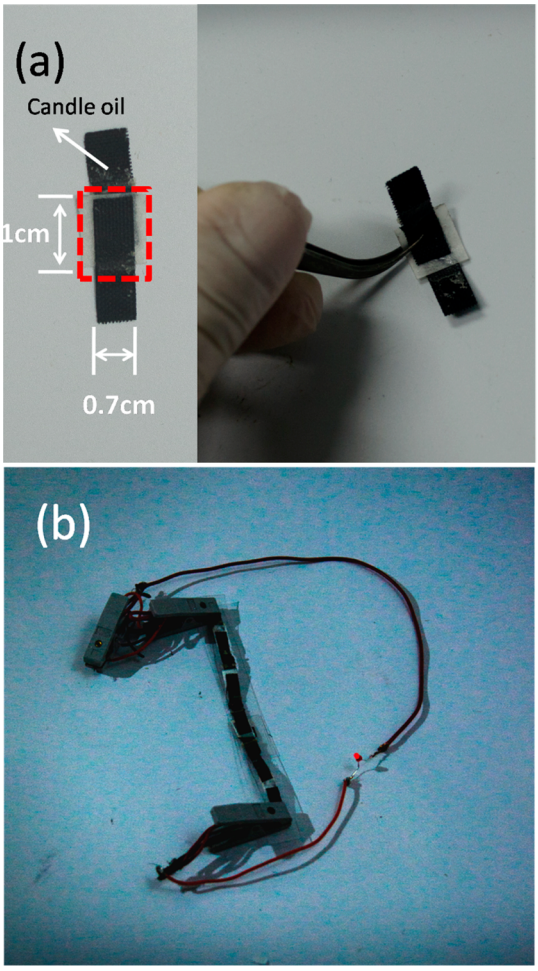

Figure 5. (a) Optical photographs of the fabricated solid-state supercapacitor device. The square in the left image indicates the capacitance region. Candle oil is used to prevent the electrolyte from immersing the electrode beyond the capacitance region. The right image demonstrates the flexibility of the device. (b) Four supercapacitor units are connected to light a light-emitting diode.

electrode. The electron diffusion between the electrolyte and VAGN may also be hindered by these excessive Co_3O_4 particles, leading to a lower C_{sp}.[12] The C_{sp} also decreases as the scan rate increases from 1 mV/s to 200 mV/s. Finally, the C_{sp} of Co_3O_4-L, Co_3O_4-M, and Co_3O_4-H reach 1617, 1128, and 602 F/g at 200 mV/s, respectively. In addition, the maximum value of the volumetric capacitance is 950 F/cm^3 (Figure S2), higher than the previous report[25,26] (Table S1).

A symmetric all-solid-state was assembled by two Co_3O_4-H electrodes, as shown in Figure 5a. The as-prepared supercapacitor is flexible and can be bent without sacrificing the electrochemical performance. Figure 6a shows that the CV chart changes slightly under different bending angles from 0° to 150°, demonstrating that the structural integrity of the device is not destroyed when folded. This performance can be attributed to the flexibility character due to the carbon fabric. On the contrary, the CV chart has a rectangular shape without the anode and cathode peaks, differing from the shape of the CV chart in the three-electrode test. Corresponding with the previous report,[11] the Co_3O_4-based hybrid electrodes are charged and discharged at a pseudoconstant rate over the entire voltammetric cycles, resulting in the absence of the redox peaks. Figure 6b shows the galvanostatic charge/discharge result. The linear profile of the charge and the discharge curves reveals the good capacitive characteristics of the solid-state supercapacitor device. As shown in Figure 6c, the device delivers high specific capacitance values of 580, 450, 350, 300, 238, and 196 F/g at discharge current densities of 1, 2, 5, 10, 20, and 40 A/g, respectively. The specific capacitance decreases as the current increases, for the same reason as the electroperformance in the three-electrode system. This is due to the fact that the high current makes more active material insufficient in the redox reaction as the scan rate increases.[23] These specific capacitance values are higher than the reported literature values for the symmetric all-solid-state supercapacitor, such as the graphene/MnO_2 ultrafilm (254 F/g at 0.5 A/g)[27] and ITO/MnO_2 nanoparticles (341.4 F/g at 0.2 mA/cm^2).[28]

The cycling stability of the supercapacitor was tested through a cyclic charge/discharge process at a current density of 20 A/g, as shown in Figure 6d. The device demonstrated an excellent stability, remaining at 86.3% of its initial capacitance after 20 000 charge/discharge cycles. No significant electrochemical changes were observed after the long-term process, as shown in the inset of Figure 6d. For the symmetric device, the energy and power densities were calculated from galvanostatic discharge curves and plotted on the Ragone diagram shown in Figure 6e. Various energy densities can be reached with various power densities: 33 Wh/kg at 10 kW/kg, 41.6 Wh/kg at 5 kW/kg, and 48.6 Wh/kg at 2.5 kW/kg. The maximum energy density of 80 Wh/kg is achieved at a power density of 0.5 kW/kg, while the highest power density is of 20 kW/kg at the energy density of 27 Wh/kg. The operating voltage window is 1 V. These values are superior to the previously reported symmetric systems graphene/MnO_2 (6.8 Wh/kg at 62 W/kg),[13] MnO_2 (18 Wh/kg at 12.6 kW/kg),[27] and graphene/MnO_2 (4.8 Wh/kg at 14 kW/kg).[15] Noteworthy, the energy density and power density are comparable in the asymmetric system of graphene/MnO_2 (7 Wh/kg at 5 kW/kg) with a voltage window of 2 V.[29] We had connected four supercapacitor units in series to light a light-emitting diode (LED) after charging to 2 V, as shown in Figure 5b. Each used device has the same area of 0.7 cm^2.

Tested in a frequency range from 0.01 Hz to 10 kHz at an open-circuit potential with an ac amplitude of 10 mV, the charge-transfer procedure of the symmetric device can be analyzed by the electrochemical impedance spectra. We also used an equivalent circuit to obtain the charge-transfer resistance (Figure 6f, inset); R_s, R_{ct}, and C_p represent the electrolyte resistance, the

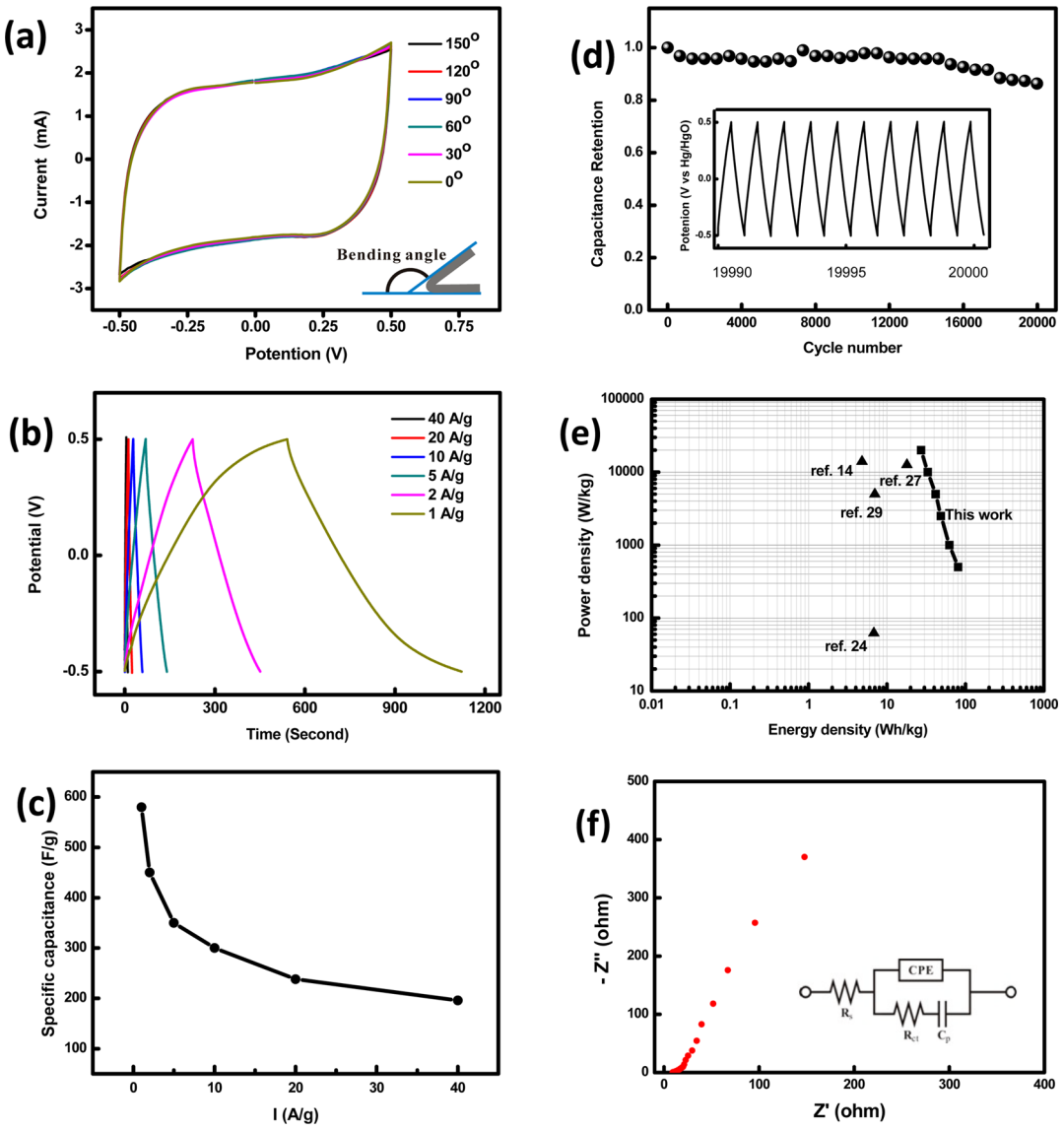

Figure 6. (a) CVs for the device at various bending angles. (b) Galvanostatic charging/discharging curves of the supercapacitor device at various current densities. (c) Specific capacitance *vs* current densities for the supercapacitor device. (d) Cycling stability of the device at 20 A/g. The inset shows the galvanostatic charge/discharge curves of the last 10 cycles. (e) Ragone plots of the supercapacitor device. The values of other reported supercapacitors are added for comparison. (f) Nyquist plot of the supercapacitor device; the inset is the equivalent circuit.

charge-transfer resistance, and the pseudocapacitive element due to the redox process of Co_3O_4, respectively.[12] CPE refers to a constant phase element due to the double-layer capacitance. The result of R_{ct} is 20.66 ohm, indicating a low internal resistance for the whole device.

CONCLUSION

A Co_3O_4/VAGN/CF hybrid structure electrode was synthesized with a high specific capacitance of 3480 F/g, close to the theoretical value. A solid-state supercapacitor was fabricated by two pieces of these electrodes. The device exhibited an excellent stability under different bending angles and long cycling. The maximum energy density of 80 Wh/kg and highest power density of 20 kW/kg demonstrated that the device has great potential applications in energy management for flexible and lightweight electronics.

EXPERIMENTAL SECTION

Synthesis of VAGN/CF. The synthesis of the VAGN was carried out in a microwave plasma enhanced chemical vapor deposition system (MPECVD) as in our previous work.[12] The rectangular microwave waveguide was coupled with the microwave power in a quartz tube for generating the plasma. A piece of carbon fabric (5 cm × 0.7 cm) was used as the substrate. The temperature of the plasma was controlled by microwave power

in H_2. The heating step started after the chamber had been evacuated to 5 mTorr. During the heating step, H_2 flowed into the chamber at a rate of 30 sccm with a microwave power of 800 W and a chamber pressure of 8.5 Torr. After reaching 385 °C, CH_4 flowed into the chamber at a rate of 30 sccm while changing the H_2 to 20 sccm. The graphene deposition procedure lasted 2.5 min. Then the carbon fabric was taken out and rolled over to deposit the graphene on the other side. The as-deposited graphene was located in the middle of the carbon fabric stretching a length of 1 cm.

Synthesis of Co_3O_4/VAGN/CF Composites. In a typical experiment to prepare the Co_3O_4/VAGN/CF composites, 2 mg of $Co(CH_3COO)_2 \cdot 4H_2O$ was dispersed in 16 mL of ethanol. A light purple solution was obtained after stirring for 10 min. The solution was then transferred into a Teflon stainless steel autoclave with a capacity of 25 mL. The as-prepared VAGN/CF was put into the solution before the autoclave was sealed and hydrothermally treated for 3 h at 150 °C. After cooling to room temperature naturally, the composites were taken out and washed repeatedly with ethanol and deionized water. The composite was annealed under vacuum at 120 °C for 10 h and then in the air at 250 °C for 3 h. The as-prepared sample was named Co_3O_4-L. The Co_3O_4-M and Co_3O_4-H were made only by changing the amount of $Co(CH_3COO)_2 \cdot 4H_2O$ to 5 and 200 mg, respectively. To calculate the mass of the Co_3O_4, the samples were dissolved in HCl solution and the concentration of Co ion in the solution was measured by the inductive coupled plasma emission spectrometer method.

Characterizations. The morphologies of the Co_3O_4/VAGN/carbon fabric were characterized by field scanning electronic microscopy (Quanta 400F) with an accelerating voltage of 20 kV. Transmission electron microscopy images were taken with a FEI Tecnai G2 F30 microscope operated at 300 kV. XPS measurements were carried out with an ESCA Lab250 spectrometer using a twin-anode Al Kα (1486.6 eV) X-ray source. All spectra were calibrated to the binding energy of the C 1s peak at 284.6 eV. The base pressure was around 3×10^{-7} Pa. The structural phases of the products were measured by powder X-ray diffraction experiments on a Rigaku X-ray diffractometer (D-MAX 2200 VPC).

Electrochemical Measurement. After the carbon fabric with graphene and Co_3O_4 had been annealed, its central part has an area of 1 cm × 0.7 cm. The other part of the carbon fabric was either cut off or covered by candle oil except the space connected with the electrochemical workstation. In the three-electrode tests, the Co_3O_4/VAGN/carbon fabric composites, the Hg/HgO electrode, and a piece of Pt electrode were used as the working electrode, the reference electrode, and the counter electrode, respectively. The electrolyte used in the electrochemical measurement was a 2 M KOH aqueous solution. In the two-electrode all-solid-state test, the electrolyte was PVA/KOH gel, prepared as follows: 3.58 g of KOH was added into 60 mL of deionized water, and then 6 g of PVA power was added. The mixture was heated to 95 °C under stirring until the solution became clear. Two pieces of Co_3O_4-H were immersed into the PVA/KOH solution for 3 min, then taken out and assembled together with a filter paper as the separator. All electrochemical tests were performed in an electrochemical workstation (IviumStat, Ivium).

Conflict of Interest: The authors declare no competing financial interest.

Supporting Information Available: The nitrogen adsorption isotherms of the VAGN; the volumetric capacitance *vs* scan rate of various composites; a list of the specific and volumetric capacitance in previous work. The Supporting Information is available free of charge on the ACS Publications website at DOI: 10.1021/acsnano.5b00821.

Acknowledgment. This work was financially supported by the National Natural Science Foundation of China (51125008, 11274392, U1401241).

REFERENCES AND NOTES

1. Hercule, K. M.; Wei, Q. L.; Khan, A. M.; Zhao, Y. L.; Tian, X. C.; Mai, L. Q. Synergistic Effect of Hierarchical Nanostructured MoO_2/$Co(OH)_2$ with Largely Enhanced Pseudocapacitor Cyclability. *Nano Lett.* **2013**, *13*, 5685–5691.
2. Kaempgen, M.; Chan, C. K.; Ma, J.; Cui, Y.; Gruner, G. Printable Thin Film Supercapacitors Using Single-Walled Carbon Nanotubes. *Nano Lett.* **2009**, *9*, 1872–1876.
3. Niu, Z.; Zhang, L.; Liu, L.; Zhu, B.; Dong, H.; Chen, X. All-Solid-State Flexible Ultrathin Micro-Supercapacitors Based on Graphene. *Adv. Mater.* **2013**, *25*, 4035–4042.
4. Huang, L.; Chen, D.; Ding, Y.; Feng, S.; Wang, Z. L.; Liu, M. Nickel-Cobalt Hydroxide Nanosheets Coated on $NiCo_2O_4$ Nanowires Grown on Carbon Fiber Paper for High-Performance Pseudocapacitors. *Nano Lett.* **2013**, *13*, 3135–3139.
5. Cheng, Y. W.; Zhang, H. B.; Lu, S. T.; Varanasiad, C. V.; Liu, J. Flexible Asymmetric Supercapacitors with High Energy and High Power Density in Aqueous Electrolytes. *Nanoscale* **2013**, *5*, 1067–1073.
6. Wu, Z. S.; Wang, D. W.; Ren, W.; Zhao, J.; Zhou, G.; Li, F.; Cheng, H. M. Anchoring Hydrous RuO_2 on Graphene Sheets for High-Performance Electrochemical Capacitors. *Adv. Funct Mater.* **2010**, *20*, 3595–3602.
7. Cao, X. H.; Shi, Y. M.; Shi, W. H.; Lu, G.; Huang, X.; Yan, Q. Y.; Zhang, Q. C.; Zhang, H. Preparation of Novel 3D Graphene Networks for Supercapacitor Applications. *Small* **2011**, *7*, 3163–3168.
8. Rakhi, R. B.; Chen, W.; Cha, D. Y.; Alshareef, H. N. Substrate Dependent Self-Organization of Mesoporous Cobalt Oxide Nanowires with Remarkable Pseudocapacitance. *Nano Lett.* **2012**, *12*, 2559–2567.
9. Wang, G. X.; Shen, X. P.; Horvat, J.; Wang, B.; Liu, H.; Wexler, D.; Yao, J. Hydrothermal Synthesis and Optical, Magnetic, and Supercapacitance Properties of Nanoporous Cobalt Oxide Nanorods. *J. Phys. Chem. C* **2009**, *113*, 4357–4361.
10. Wang, L.; Liu, X. H.; Wang, X.; Yang, X. J.; Lu, L. D. Electrochemical Capacitance Study on Co_3O_4 Nanowires for Super Capacitors Application. *J. Mater. Sci: Mater. Electron.* **2011**, *22*, 601–606.
11. Yang, L.; Cheng, S.; Ding, Y.; Zhu, X.; Wang, Z. L.; Liu, M. Hierarchical Network Architectures of Carbon Fiber Paper Supported Cobalt Oxide Nanonet for High-Capacity Pseudocapacitors. *Nano Lett.* **2012**, *12*, 321–325.
12. Liao, Q. Y.; Li, N.; Cui, H.; Wang, C. X. Vertically-Aligned Graphene@MnO Nanosheets as Binder-Free High-Performance Electrochemical Pseudocapacitor Electrodes. *J. Mater. Chem. A* **2013**, *1*, 13715–13720.
13. He, Y. M.; Chen, W. J.; Li, X. D.; Zhang, Z. X.; Fu, J. C.; Zhao, C. H.; Xie, E. Q. Freestanding Three-Dimensional Graphene/MnO_2 Composite Networks as Ultra light and Flexible Supercapacitor Electrodes. *ACS Nano* **2013**, *7*, 174–182.
14. Wang, X.; Liu, B.; Liu, R.; Wang, Q.; Hou, X.; Chen, D.; Wang, R.; Shen, G. Fiber-Based Flexible All-Solid-State Asymmetric Supercapacitors for Integrated Photodetecting System. *Angew. Chem.* **2014**, *53*, 1849–1853.
15. Yuan, L. Y.; Lu, X. H.; Xiao, X.; Zhai, T.; Dai, J. J.; Zhang, F. C.; Hu, B.; Wang, X.; Gong, L.; Chen, J.; Hu, C. G.; Tong, Y. X.; Zhou, J.; Wang, Z. L. Flexible Solid-State Supercapacitors Based on Carbon Nanoparticles/MnO_2 Nanorods Hybrid Structure. *ACS Nano* **2012**, *6*, 656–661.
16. Dong, Y. M.; He, K.; Yin, L.; Zhang, A. M. A Facile Route to Controlled Synthesis of Co_3O_4 Nanoparticles and Their Environmental Catalytic Properties. *Nanotechnology* **2007**, 18.
17. Yuan, C. Z.; Yang, L.; Hou, L. R.; Shen, L. F.; Zhang, X. G.; Lou, X. W. Growth of Ultrathin Mesoporous Co_3O_4 Nanosheet Arrays on Ni Foam for High-Performance Electrochemical Capacitors. *Energ Environ. Sci.* **2012**, *5*, 7883–7887.
18. Sun, H. T.; Sun, X.; Hu, T.; Yu, M. P.; Lu, F. Y.; Lian, J. Graphene-Wrapped Mesoporous Cobalt Oxide Hollow Spheres Anode for High-Rate and Long-Life Lithium Ion Batteries. *J. Phys. Chem. C* **2014**, *118*, 2263–2272.
19. Li, X. B.; Yang, S. W.; Sun, J.; He, P.; Pu, X. P.; Ding, G. Q. Enhanced Electromagnetic Wave Absorption Performances of Co_3O_4 Nanocube/Reduced Graphene Oxide Composite. *Synth. Met.* **2014**, *194*, 52–58.
20. Liao, M. X.; Liu, Y. F.; Hu, Z. H.; Yu, Q. Novel Morphologic Co_3O_4 of Flower-Like Hierarchical Microspheres as Electrode Material for Electrochemical Capacitors. *J. Alloys Compd.* **2013**, *562*, 106–110.

21. Yan, D. L.; Zhang, H.; Chen, L.; Zhu, G. S.; Li, S. C.; Xu, H. R.; Yu, A. B. Biomorphic Synthesis of Mesoporous Co_3O_4 Microtubules and Their Pseudocapacitive Performance. *ACS Appl. Mater. Interfaces* **2014**, *6*, 15632–15637.
22. Barbieri, E. M. S.; Lima, E. P. C.; Lelis, M. F. F.; Freitas, M. B. J. G. Recycling of Cobalt from Spent Li-Ion Batteries as Beta-$Co(OH)_2$ and the Application of Co_3O_4 as a Pseudocapacitor. *J. Power Sources* **2014**, *270*, 158–165.
23. Guo, D.; Luo, Y.; Yu, X.; Li, Q.; Wang, T. High Performance $NiMoO_4$ Nanowires Supported on Carbon Cloth as Advanced Electrodes for Symmetric Supercapacitors. *Nano Energy* **2014**, *8*, 174–182.
24. Vijayakumar, S.; Ponnalagi, A. K.; Nagamuthu, S.; Muralidharan, G. Microwave Assisted Synthesis of Co_3O_4 Nanoparticles for High-Performance Supercapacitors. *Electrochim. Acta* **2013**, *106*, 500–505.
25. Dall'Agnese, Y.; Lukatskaya, M. R.; Cook, K. M.; Taberna, P. L.; Gogotsi, Y.; Simon, P. High Capacitance of Surface-Modified 2D Titanium Carbide in Acidic Electrolyte. *Electrochem. Commun.* **2014**, *48*, 118–122.
26. Lee, S. W.; Kim, J.; Chen, S.; Hammond, P. T.; Shao-Horn, Y. Carbon Nanotube/Manganese Oxide Ultrathin Film Electrodes for Electrochemical Capacitors. *ACS Nano* **2010**, *4*, 3889–3896.
27. Peng, L. L.; Peng, X.; Liu, B. R.; Wu, C. Z.; Xie, Y.; Yu, G. H. Ultrathin Two-Dimensional MnO_2/Graphene Hybrid Nanostructures for High-Performance, Flexible Planar Supercapacitors. *Nano Lett.* **2013**, *13*, 2151–2157.
28. Xue, M. Q.; Xie, Z.; Zhang, L. S.; Ma, X. L.; Wu, X. L.; Guo, Y. G.; Song, W. G.; Li, Z. B.; Cao, T. B. Microfluidic Etching for Fabrication of Flexible and All-Solid-State Micro Supercapacitor Based on MnO_2 Nanoparticles. *Nanoscale* **2011**, *3*, 2703–2708.
29. Wu, Z. S.; Ren, W. C.; Wang, D. W.; Li, F.; Liu, B. L.; Cheng, H. M. High-Energy MnO_2 Nanowire/Graphene and Graphene Asymmetric Electrochemical Capacitors. *ACS Nano* **2010**, *4*, 5835–5842.